Research Article

Ramin Jamali, Farzaneh Nazari, Azadeh Ghaffari, Sabareesh K. P. Velu, and Ali-Reza Moradi*

Speckle Tweezers for Manipulation of High and Low Refractive Index Micro-particles and Nano-particle Loaded Vesicles

Abstract: Several fundamental research and applications in biomedicine and microfluidics often require controlled manipulation of suspended micro and nanoscale particles. Speckle tweezers (ST) by incorporating randomly distributed light fields have been used to control microparticles with refractive indices higher than their medium and to perform manipulation tasks such as guiding and sorting. Indeed, compared to periodic potentials, ST represents a wider possibility to be operated for such tasks. Here, we extend the usefulness of ST into micro-particles of low index with respect to the surrounding. Repelling of such particles by high intensity regions into lower intensity regions makes them to be locally confined, and the confinement can be tuned by changing the average grain intensity and size of the speckle patterns. Experiments on polystyrenes and liposomes validate the procedure. Moreover, we show that ST can also manipulate the nanoparticle (NP)-loaded liposomes. Interestingly, the different interactions of NP-loaded and empty liposomes with ST enables collective manipulation of their mixture using the same speckle pattern, which may be explained by inclusion of the photophoretic forces on NPs. Our results on the different behavior between empty and non-empty vesicles may open a new window on controlling collective transportation of drug micro-containers along with its wide applications in soft matter.

Keywords: Optical tweezers; Speckle tweezers; Collective manipulation; Low index particles.

Ramin Jamali, Department of Physics, Institute for Advanced Studies in Basic Sciences (IASBS), Zanjan 45137-66731, Iran
Farzaneh Nazari, Department of Physics, Yazd University, Yazd 89195-741, Iran
Azadeh Ghaffari, Department of Food and Drug Control, School of Pharmacy, Zanjan University of Medical Sciences, Zanjan 45139-56111, Iran
Sabareesh K. P. Velu, Department of Physics, Rathinam College of Arts and Science, Coimbatore 641021, Tamilnadu, India
***Corresponding author: Ali-Reza Moradi,** Department of Physics, Institute for Advanced Studies in Basic Sciences (IASBS), Zanjan 45137-66731, Iran, & School of Nano Science, Institute for Research in Fundamental Sciences (IPM), Tehran 19395-5531, Iran, Email: moradika@iasbs.ac.ir

1 Introduction

Using light to control the motion of micro- and nanostructured objects is a challenge and involves several scientific and technological fields such as optical tweezing [1], Van der Waals and Casimir interactions [2, 3], integrated optics [4], biophysics [5], etc. However, in more complex light-activated devices the unavoidable disorder induces some effects including multiple-scattering, diffusion, and localization of light [6–8]. The disorder can be externally controlled, which leads to applications such as tunable lasers, transmission of light through random media, and novel disorder driven devices, such as ultrasensitive spectrometers [7, 9, 10]. Yet, there is a specific field -optomechanics- in which the beneficial features of randomness have not been sufficiently investigated. Optomechanical forces come from the interaction of the electromagnetic wave with the boundaries of dielectric objects. On the other hand, random systems include a large number of boundaries for which calculation of the forces is not trivial, but it is crucial to understand the mechanisms of optically activated devices [11].

Several fundamental researches and applications in biomedicine and microfluidics often require controlled manipulation of micro and nanoscale particles suspended in a fluidic medium [12]. The conventional strategy is to trap particles utilizing optical trapping forces [1], photoacoustic effects [13], and magnetic and electric forces [14]. Progressions into a specific approach has resulted in numerous breakthroughs in pharmaceutics and microfluidics [15–17]. A primary advantage of specific methodology is the opportunity for it to be applied in the manipulation of drug containers in targeted drug delivery [18]. Among various approaches, optical tweezers have been particularly prosperous due to their inherent versatility. Optical trapping of micron-sized particles was introduced by A. Ashkin [19]. Since then, it has been successfully implemented in two size ranges: the subnanometer scale for cooling of atoms, ions and molecules [20, 21], and the micrometer scale for non-invasive manipulation of microscopic ob-

jects such as cells and bacteria [22]. Further developments through externally controlling the position and stiffness of individual trap sites, offer manipulation tasks in parallel and lead to many important breakthroughs in bioscience, materials science, microfluidics, and soft condensed matter physics [23]. Conventional optical traps require careful engineering and aligning of setups and sample preparation. Therefore, such stringent conditions are not matchable with the simplicity, low-cost and high-throughput requirements that are necessary for biomedical applications.

The light gradient force exerted on a dielectric particle must overcome the scattering force for steady trapping, especially along the axial direction. The gradient force acting on the particle is proportional to $\pm\nabla E^2$, where E is the electric field of the beam, and the difference in the refractive indices between the surrounding medium n_m and the particle n_p indicates the sign. The realization of stable trapping of high-refractive-index particles is easy since the intensity profile of tightly focused laser beams with a spatially homogeneous state of polarization is in the form of a Gaussian distribution. However, for low-refractive-index particles, i.e., when the refractive index of the particle is lower than that of the surrounding medium ($n_p < n_m$), the gradient force will point from the focus center to the region of low-intensity and will repel the particle away from the highest intensity point. Therefore, low-index (with respect to the surrounding) particles require a different strategy to be manipulated by optical tweezers; to trap them, a beam with a focusing feature of hollow intensity distribution, the so-called hollow beam, is used. Various types of hollow beams, such as high order Bessel beams, Laguerre-Gaussian beams, azimuthally polarized beams, and the output beam of small hollow fibers, etc. have been tested and applied for this purpose in recent years [24–26]. The hollow shaped beams, can alternatively be achieved using a circularly scanning optical tweezers [27]. This technique, indeed, offers further advantages over the aforementioned structured beams, such as the ease and speed with which the geometry of the trapping potential can be varied [28]. Trapping by hollow beams, furthermore, results in a reduction of possible photo-damage, which is crucial for biological specimens [29].

On the other hand, it is known that low-refractive-index (with respect to the surrounding) particles have an important role in physics, medicine, and technology. For example, trapping a single gas bubble in water in an acoustic resonant cavity has allowed several studies to understand the physics of sonoluminescence [30] and to establish further applications in biology and medicine. More importantly, the bubbles are used to enhance the contrast of images in ultrasound imaging [31]. Besides bubbles, low-refractive-index (with respect to the surrounding) particles are found in water-in-oil emulsions for petroleum, and food processing applications [32]. Another important class of low-index particles are liposomes. A liposome is a spherical vesicle with a molecularly thin and self-assembled membrane, and may act as an appropriate container for nutrients and pharmaceutical medicines in drug delivery [33] and can be applied to enhance the transfection of genes into living cells [34, 35]. Liposomes are made of phospholipids and are developed by disrupting biological membranes, their most important kind being the multilamellar vesicles [36].

Usually, it is difficult to optically trap both kinds of particles (low and high-refractive-indices with respect to their surrounding) as it requires complex scanning methods and/or rigorous design of holographic tweezers [37–40]. Therefore, conventional methods are not suitable for more complex micro-manipulation tasks such as transportation of a large number of such mixtures of particles. Also, limitations such as the short working distance of high numerical aperture microscope objectives undermine the efficiency of the methods. On the one hand, for many of the applications, especially when dealing with collective motion of microscopic objects, the regular arrays of trap sites are no more required. On the other hand, for several applications, again especially the ones that deal with collective motions, brief and local confining of the objects is sufficient, and a tight optical trapping is no more a requirement. In this paper, we propose the use of speckle tweezers (ST) as an elegant alternative such cases. ST possesses both the simplicity and applicability in optical manipulation of real-life situations. Speckle light patterns are high-contrast, fine-scale granular patterns that are the result of the interference of a large number of dephased but coherent monochromatic light waves propagating along different directions [41]. Speckle patterns can be generated through different processes, such as scattering of laser light from a rough surface or mode-mixing in a multimode fiber [42]. It has been demonstrated that ST is a versatile tool to efficiently perform collective optical manipulation tasks, such as trapping, guiding, and sorting of high-refractive-index particles [43, 44]. Although, the intrinsic randomness of speckle patterns is considered to be a disturbing noise in experiments, nevertheless, the patterns find several useful applications. One of the first experiments on the use of ST in this range demonstrated the emergence of anomalous diffusion in colloids and showed the control of the motion of Brownian particles [45]. Recently, the optical speckle field has been used for producing a thermal speckle field through interaction with plasmonic substrates and converting the high-intensity speckle grains into the cor-

responding thermal speckle grains [46]. In another recent study, it has been shown that the density of the structural defects in a 2D binary colloidal crystal can be engineered using a speckle field [47]. A memory equation based on a theoretical model was provided to describe the motion of colloidal particles within the ST field [48, 49]. The speckle field contains a random, but somehow tunable, distribution of isolated high-intensity regions surrounded by irregular and interconnected low-intensity regions, and the dark spots are, indeed, much more common than bright ones [50–52]. This nature of the speckle fields makes the use of ST as an elegant possibility for collective manipulation of mixtures of low and hight index (with respect to the surrounding) micro-particles. Regions with higher and lower intensities in the speckle field can be used to confine the high-refractive-index and low-refractive-index particles with respect to their surrounding, respectively. Moreover, by examination of speckle fields effect on not-empty but nano-particle (NP) loaded liposomes, we experimentally corroborate that the ST may be used to perform control on the collective movement of drug micro-containers.

2 Materials and methods

2.1 Sample preparation

Liposomal of clindamycin phosphate (CP) is prepared by thin-film hydration method. CP is purchased from Suzhou Pharmaceutical. Monobasic potassium phosphate (98- 100.5%), phosphoric acid (85-88%), sodium hydroxide (>98%), Tween 80 (for synthesis), triton X-100 (99%) and high performance liquid chromatography HPLC-grade acetonitrile are purchased from Merck. Sephadex G-50 is purchased from MilliporeSigma. Egg phosphatidyl cholin (E80) is purchased from Lipoid. Cholestrol (99%) is purchased from Sigma-Aldrich. The lipid mixture is dissolved in chloroform/methanol (2:1) and get dried under a reduced pressure in a rotary evaporator at 60°C to form a thin lipid film. The film is then hydrated with CP solution (63 mg/ml) in phosphate buffer solution pH = 7.4 at 60°C for 1 hour.

The synthesis of liposomes can be achieved by various methods and their created sizes depend on the involved parameters and materials [53]. In general, the liposome size can vary from very small (0.025 μm) to large (2.5 μm) vesicles. Moreover, liposomes may have one or more bilayer membranes. The vesicle size is an acute parameter to determine the circulation half-life of the liposomes. In the thin-film hydration methodology that we use in our experiments, we consider the parameters toward creating the liposomes in the range of 1 μm sizes. Further, we separate out the liposomes of 1 μm by multiple passing of lipid suspension through the syringe filter (Sterlitech) to ensure of sufficient uniformity. We determine the size distribution of liposomes by laser diffraction method (Mastersizer 2000, Malvern Instruments) which shows a sufficient homogeneity for multiple trapping experiments. This apparatus provided a mean diameter of 1 μm associated with a standard deviation of ±38 nm. These liposomes are in multilamellar vesicles class, i.e., their structures consist of concentric phospholipid spheres separated by layers of water. The refractive index of the formed liposomes is 1.300, which is measured by Abbe refractometer (Atago, NAR-1T). Zeta potentials of the liposomes are determined at room temperature in deionized water with a Malvern Zetasizer Nano ZS (Malvern Instruments). The zeta potentials of liposomes are measured to be in the range of -10.9 to -11.4 mV. Encapsulation efficiencies of liposomes are calculated to be 20.8% in day 0. The short-time stability of liposomes in term of encapsulation efficacy is studied for one week. The encapsulation efficacy in day 1 and day 7 are measured as 11.4% and 12.1%, respectively. The preparation of liposome samples results in a high concentration solution of liposomes. The viscosity of the stock solution is 340×10^{-3} Ns/m^2, measured by a commercial rotational viscometer (ViscoQC 100, Anton Paar). For trapping experiments, similar to trapping experiments of the polystyrene particles, a very dilute solution in distilled water is prepared which has a similar viscosity value (η_l=0.0012 Ns/m^2) to the viscosity of polystyrene solution (η_w=0.001 Ns/m^2).

Gold NPs of 100±5 nm diameter and optical density of 1, and polystyrene particles of 1 μm diameter are purchased from Sigma-Aldrich. Citrate buffer, which is a proprietary surfactant is used as a stabilizer for NPs. Gold NPs are loaded passively to the liposomes i.e. encapsulated during the liposome formation. To this end, during the liposome preparation and in the hydration stage, 100 microliter of gold NPs are added to distilled water. Before the experiments, polystyrene particles, liposomes, and the NP-loaded liposomes are shaken for a few minutes by an ultrasonic bath (Xuba3, Grant), and separate dilute solutions of them, which are suitable for trapping experiments, are prepared. The concentration could be further adjusted by the use of a push-pull syringe pump, connected into the surrounding medium and the high concentrate liposome reservoirs. For example, for increasing the concentration, we infuse the liposomes directly into the chamber and withdraw the surrounding medium at the constant rate.

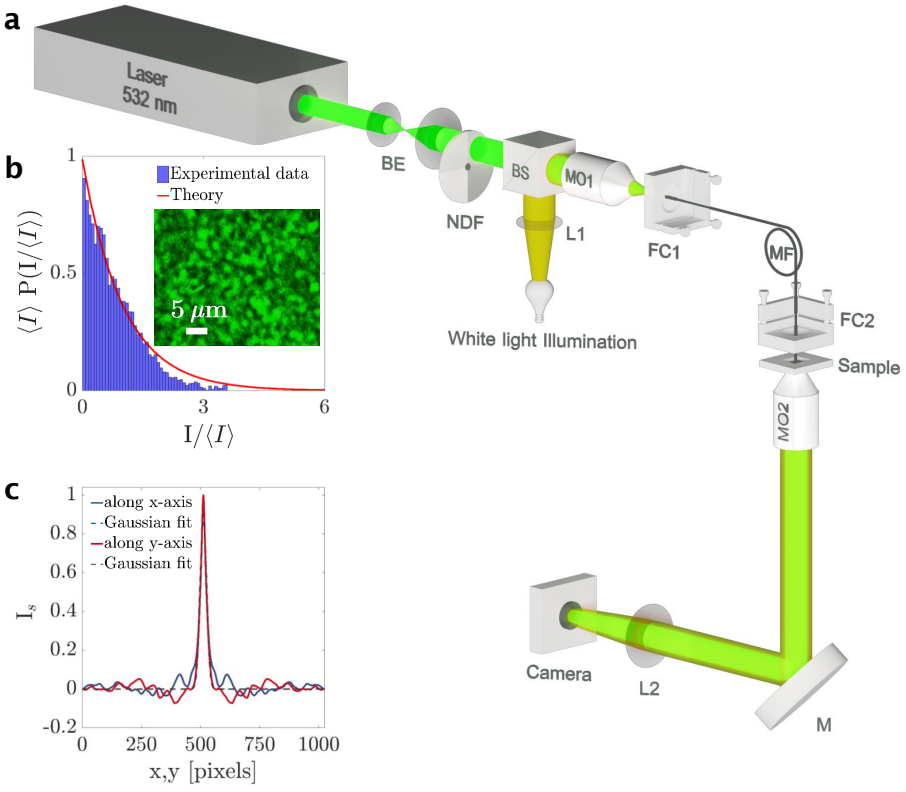

Fig. 1: (a) Schematic of the experimental setup; BE: beam expander, MO: microscope objective, MF: multi-mode fiber, NDF: neutral density filter, BS: beam splitter, FC: fiber coupler, L: lens, M: mirror. (b) Intensity distribution of the speckle pattern at the sample plane and negative exponential function fitting. Blue bars demonstrate the experimental data and red solid line shows the theoretical probability density function, which follows the negative exponential distribution. Inset: A microscopy image of the speckle pattern. (c) Normalized speckle pattern intensity spatial auto-correlation function I_s as a function of position. The blue and red lines are speckle intensity along x and y axis, respectively, and the dashed blue and red lines are their corresponding Gaussian functions. The average speckle grain size is determined from the standard deviation of the Gaussian function. In our case, the average speckle grain size is 1.69 ± 0.20 μm. In our configuration 1 pixel equals to 0.052 μm.

We fabricate special chambers with a couple of glass coverslips (22 × 22 mm, thickness of 170 ± 5 μm) and parafilm spacers, in which parts of one of the building coverslips are coated by a semi-transparent layer, for reducing the transmittance of the laser light up to 15%. The coating is performed using Sliver (Ag) sputter targets in a sputter coater system (DST3-A, Nanostructured Coatings Co.) on the pre-covered areas of the coverslip. By tuning the coating duration and the applied voltage the transmittance of the coated area can be tuned.

2.2 Experimental Procedure

Figure 1**a** shows the schematic of the home-built STs experimental setup to perform the experiments. A laser beam (DPSS, 85-GSS-309, Melles Griot, 532 nm) is expanded by the beam expander (BE) and by the use of a microscope objective (MO1, 10×, NA = 0.25) is focused onto the input entrance of a multi-mode fiber (MF, QMMF, OZ Optics). A step-variable neutral density filter (NDF) is used to reduce the beam intensity in steps. A beam splitter (BS) is also used to direct a white light illumination along with laser light into the sample for conventional microscopic imaging. The multi-mode fiber has a core diameter of 365 ± 14 μm, numerical aperture of NA = 0.22, and core and cladding refractive indices of 1.4589 and 1.4422, respectively. Therefore, our MF can mix up to approximately 474 modes of the propagating laser beam, and the output light from the fiber is the interference of several modes with random phases and results in generating the speckle pattern at the sample plane. The microscope objective MO2 (40×, NA = 0.65), mirror (M), and the lens (L2) form the image of the sample on the camera (DCC1545M, Thorlabs, 5.2 μm pixel pitch). The sample chamber consists of a microfluidic channel with

an inlet and outlet to inject, withdraw, or flow aqueous samples by the use of a syringe pump (NE-300, Just Infusion™). The details of the sample chambers are presented in Supplementary Fig. S1 and a discussion on choosing the proper speckle field generation method is provided in Supplementary Fig. S2.

Figure 1**b** shows the theoretical (red color solid line) and experimental (blue color bars) probability density function of a typical speckle pattern at the sample plane. In its inset a microscopy image of the speckle pattern as observed on the camera is shown. The average grain size of the speckle field in this pattern is 1.69 μm and the average speckle intensity is $\langle I \rangle = 5.46\ \mu\mathrm{W}/\mu\mathrm{m}^2$. The experimental data is obtained by averaging the intensity distribution of 1000 speckle patterns. The probability density function of the speckle pattern intensity follows the negative exponential (Gamma with parameter 1) distribution, i.e., $\frac{1}{\langle I \rangle} \exp\left(-\frac{I}{\langle I \rangle}\right)$ [42, 54]. Figure 1**b** shows a good agreement between theory and the distributions of the speckle pattern intensities used in the experiments, which confirms that the speckle patterns used in the experiments are well-formed.

Figure 1**c** shows the auto-correlation function of the speckle pattern intensity. The average speckle grain size is determined by evaluating the normalized spatial autocorrelation function on our 2D imaged speckle images by digital video microscopy. The resulted normalized 2D intensity autocorrelation function (blue and red solid lines in Fig. 1**c** for x and y, respectively) is then fitted by the Gaussian function along x-axis (blue dotted line in Fig. 1**c**) and y-axis (red dotted line in Fig. 1**c**) to obtain the standard deviation. The obtained standard deviations along x-axis and y-axis are averaged to calculate the average speckle grain size. In Supplementary Fig. S2 we show how the grain size depends on the wavelength and the geometry of the speckle generating system. The maximum power of the laser used in our experiments at the output of the laser is 250 mW, which after passing through BS and MO1 is reduced to 100 mW at the entrance of the optical fiber. The output power of the optical fiber can be obtained from $A = \frac{10}{L} \log \frac{P_{in}}{P_{out}}$, where A is the maximum attenuation and L is the length of the multimode fiber, and P_{in} and P_{out} are its input and output power, respectively. In our experiments we used an optical fiber of $L = 50$ cm length which has an attenuation coefficient of $A = 5.5$ dB/km. Therefore, the total power exiting from the fiber is 99.94 mW, almost the same at the entrance without any attenuation. This power is propagated by 1 cm to the sample and the diameter of the illumination area can be calculated having the NA of the fiber. NA=0.22 gives the diameter of the area as 4.5 mm. Therefore, the average intensity over the illuminated area will be 6.2 $\mu\mathrm{W}/\mu\mathrm{m}^2$. The power of the laser entering to the fiber was 88 mW, for which, considering the aforementioned procedure the calculated average speckle intensity is 5.46 $\mu\mathrm{W}/\mu\mathrm{m}^2$.

3 Results and Discussion

To demonstrate trapping and the manipulation of low-refractive-index (with respect to the surrounding) particles using a speckle field we start by considering the motion behavior of two samples containing polystyrene microspheres (diameter of 1 μm, refractive index of $n_p = 1.59$) and liposome vesicles (diameter of 1 μm, refractive index of $n_l = 1.30$) under the exposure of randomly distributed laser field. We brought the output end of a multimode fiber into the specimen chamber to impose the speckle field on the dispersed particles. The average intensity of the speckle grains is controlled by tuning the intensity of the laser light, and the grain size can be varied by careful adjustment of the fiber end to sample distance. The microfluidic chamber is connected to an infusion pump to infuse the micro-particles and allow them to flow (infusion rate = 1.25 ml/hr). First, in separate experiments, we imposed the speckle field on multiple low- and high-refractive-index particles in a quiescent medium ($n_m = 1.33$). Figures 2**a** and 2**b** show the path trajectories of the typical low- and high-refractive-index (with respect to their surrounding) particles, respectively, for the different speckle field strengths. As the trajectories show, polystyrene beads reposition themselves in the bright regions of the speckle pattern and under strong optical forces ($\langle I \rangle = 5.46\ \mu\mathrm{W}/\mu\mathrm{m}^2$) they remain trapped in one of the speckle bright grains for several minutes. However, according to their Brownian motion, the particles can also move inside the speckle grain. By reducing the average laser intensity to $\langle I \rangle = 3.24\ \mu\mathrm{W}/\mu\mathrm{m}^2$ they are still trapped but can move between the neighboring grains. By further reducing the average intensity ($\langle I \rangle = 1.08\ \mu\mathrm{W}/\mu\mathrm{m}^2$) the optical forces become relatively low and the particles may show almost free diffusion but still feel the speckle field. Similar behavior is observed in liposome vesicles. However, predictably, according to their low-refractive-index with respect to their surrounding medium, as the trajectories of Fig. 2**b** show, the liposomes are restricted to the dark regions of the speckle field. Eventually when the average intensity reduces to $\langle I \rangle = 1.08\ \mu\mathrm{W}/\mu\mathrm{m}^2$ the liposomes can move between several dark regions. The optical force vector acting on a moving particle moves in the speckle field and varies with a characteristic time scale, which is

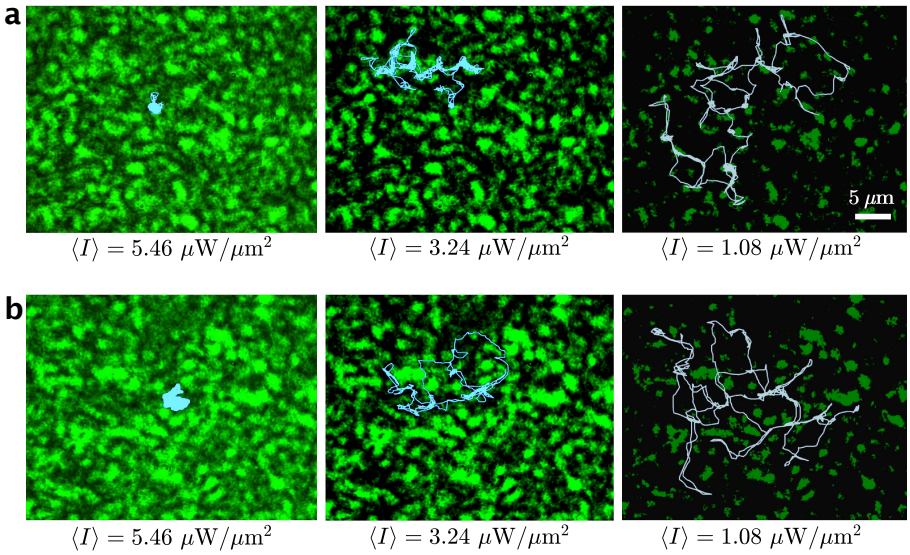

Fig. 2: The experimental trajectories (turquoise solid lines) of high and low-refractive-index (with respect to their surrounding) particles in regressive confinement through decreasing the average speckle intensity ($\langle I\rangle = 5.46\ \mu\mathrm{W}/\mu\mathrm{m}^2$, $\langle I\rangle = 3.24\ \mu\mathrm{W}/\mu\mathrm{m}^2$, $\langle I\rangle = 1.08\ \mu\mathrm{W}/\mu\mathrm{m}^2$) for the duration of 1000 s. The surrounding medium is distilled water of refractive index $n_m = 1.33$, viscosity of $\eta_w = 0.001\ \mathrm{Ns/m}^2$ at temperature $T = 300$ K. The background represents the speckle field generated by propagating of a solid state laser light through a multimode fiber. (a) Trajectories of a polystyrene particle of diameter $D_p = 1\ \mu$m and refractive index of $n_p = 1.59$. (b) Trajectories of a liposome vesicle of diameter $D_l = 1\ \mu$m and refractive index of $n_l = 1.30$.

inversely proportional to the average speckle intensity in the first approximation [43]. The motion of a Brownian particle in a static speckle field is the result of random thermal forces and deterministic optical forces. However, the optical forces are the main forces in these experiments. They attract high-index (with respect to the surrounding) particles towards the intensity maxima of the optical field but repel the low-index (with respect to the surrounding) ones to the outer sides of the speckle grains resulting in trapping them in the dark regions. The optical forces act on both high- and low-index (with respect to their surrounding) particles stumbling in the speckle field in a characteristic time, the so-called waiting time, which is defined as the time that the particle moves along its correlation length with its average drift speed [43]. The average particle drift speed is directly proportional to the average force and inversely to its friction coefficient. It has shown that even a random optical field, regardless of its inherent randomness, may be used to control the motion of the high-index particle [43]. For a low-index (with respect to the surrounding) particle, this is performed through repelling it by the speckle grains.

For the particle in a static speckle pattern, when the optical forces are relatively low the particle is almost freely diffusing away from a speckle grain before experiencing the influence of the optical forces. Increasing the forces, a subdiffusive behavior is shown and the high (low) index with respect to the surrounding particle is constrained in the bright (dark) grains. However, the particle has small probability to escape a speckle grain and can still move between the neighboring grains. At strong forces, the particle remains trapped in one of the bright or dark speckle grains, depending on the particle refractive index. In Supplementary movie S2 the videos and the overlaid trajectories of the low and high refractive index (with respect to the surrounding) particles in the speckle field are embedded.

The mean square displacement (MSD) of the particle motion is a quantitative expression to describe the aforementioned behavior of the particle inside the speckle field, and is defined as $\mathrm{MSD}(\Delta t) = \langle \Delta r^2(\Delta t)\rangle = \langle [r_j(t_0+\Delta t) - r_j(t_0)]^2\rangle_{j,t_0}$, where $r_j(t)$ denotes the position of micro-particles j at time t, and the average is derived over all micro-particles j and all onset time t_0. It means that, we consider both the ensemble and time average. Figures **3a**, **3b**, and **3c** show the MSD of a polystyrene particle, a liposome, and a liposome containing NPs, respectively, that are moving in a static speckle field of different average speckle intensities. Every MSD curve is obtained by averaging over 1000 different trajectories for the time duration of 1000 s, and the frame rate of the acquisition camera is set to 25 fps. The trajectories are for

different particles that can be found in the field of view. It happens that in the field of view a set of particles appear and get tracked, and then we change the field of view to find another set of particles. This procedure continues to obtain over 1000 trajectories and from the averaging the associated MSD curve for the specified mean intensity and particle type is achieved.

In the absence of optical forces or for low optical forces and for longer times, the MSD behaves almost linearly with Δt (MSD $\sim 4D_{\mathrm{SE}}\Delta t$, where D_{SE} is the Stokes-Einstein diffusion coefficient). As the forces increase and t decreases, there is a transition into a subdiffusive regime characterized by MSD $\propto \Delta t^{\beta}$ with $\beta < 1$. For a very large Δt, the motion returns into the diffusive regime, i.e., $\beta = 1$, with a smaller effective diffusion coefficient D_{eff}. Under higher external speckle forces, after the waiting time, the particle takes a rest time until bounded in another speckle grain. For even higher forces the particles cannot transit from one speckle grain to another. This behavior and diffusion-to-subdiffusion transition are very similar for all the examined particles; the low-index (with respect to the surrounding) ones are restricted to darker regions according to their trajectories. To demonstrate the acting optical forces on a low-refractive-index (with respect to the surrounding) particle in a speckle light field, we obtain the 2D microscopic force fields through force reconstruction via the maximum-likelihood-estimator analysis (FORMA) algorithm in its 2D form, which is introduced in [55]. In FORMA the forces are retrieved by the analysis of the particles' Brownian trajectories. The optical force fields generated by speckle patterns are larger extended force fields and the equilibrium positions are not known *a priori* due to their random appearance and include non-conservative components. FORMA estimates accurately the conservative and non-conservative components of the force field simultaneously with important advantages over the common methods that obtain the forces by analyzing their influence on the particles' Brownian motion. This method is more accurate, does not need calibration fitting parameters, executes much faster, and requires much fewer data. In Figs. 4**a** and 4**b** the results of the force field reconstruction in the speckle field are shown for the high- and low-refractive-index (with respect to their surrounding) particles, respectively. The green color background is the overlaid images of the speckle field pattern, whose intensity is proportional to the potential depth of the optical potential felt by the micro-particles. The red arrows plot the 2D force field exerted on the micro-particles and measured with FORMA. The trajectories (thin turquoise lines) are acquired experimentally for the motion of a polystyrene particle of diameter $D_p = 1$ μm and refractive index of $n_p = 1.59$ (Fig. 4**a**) and liposome vesicle of diameter $D_l = 1$ μm, refractive index of $n_l = 1.30$, viscosity of $\eta_l = 0.0012$ Ns/m^2 (Fig. 4**b**) in distilled water of refractive index $n_m = 1.33$, viscosity of $\eta_w = 0.001$ Ns/m^2, and at temperature $T = 300$ K. As illustrated in Fig. 2, a polystyrene (a liposome) explores the high (low) intensity regions while being trapped for a while in each bright (dark) grains before crossing over a neighbor one. We have verified these results on simulated data considering the same physical parameters of the experiments (Figs. 4**c** and 4**d**). The results of our simulations are in very good agreement with the results of the experiments. The motion of a Brownian particle in a static speckle field without fluid flow is the result of random thermal forces and the gradient optical forces, which attract high-refractive-index particles towards the intensity maxima of the optical field and, on the contrary, repel the low-refractive-index (with respect to the surrounding) ones to the intensity minima. The motion of a Brownian particle in presence of an external potential, such as a speckle pattern, can be modeled by solving the Langevin equation [43, 56], in which the inertial effects in the motion of the particle are usually neglected. The concentration of the micro-particles in our experiments, similar to usual optical trapping experiments, is low. Therefore, the effect of hydrodynamical and mechanical interactions between the dispersed particles is negligible.

The details of the force fields of the high- and low-refractive-index (with respect to the surrounding) simulated particles (Figs. 4**c** and 4**d**) moving in speckle fields show very good agreement with the experimental data. As it is shown, the magnitude of the acting force vectors on the high-index (with respect to the surrounding) particles is comparable with the one of low-index (with respect to the surrounding) particles in any typical point within the speckle field, both in experimental (Figs. 4**a** and **b**) and simulated (Figs. 4**c** and **d**) force fields. The force fields of the simulated data are obtained through the ray optics approach [57, 58]. For both the low and high refractive index (with respect to the surrounding) particles in the speckle field the dominant acting forces are the deterministic optical gradient forces and the random thermal forces. When a particle moves in the speckle field, the optical forces change both in magnitude and direction with a characteristic time scale that in first approximation is inversely proportional to the average speckle intensity [57]. These changes can be tracked having the intensity profile throughout the speckle field and employing the geometrical optics approach to form the force fields [58]. The laser beam is decomposed into a set of optical rays. As the rays reach the particle, they get partially reflected

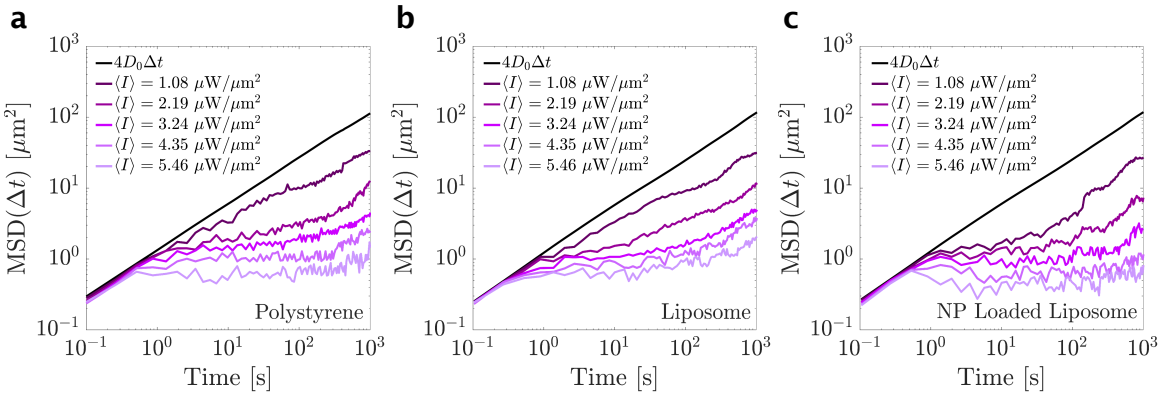

Fig. 3: Mean square displacement of Brownian particles on a logarithmic scale as a function of time in increasing speckle field intensity, for (a) a polystyrene, (b) a liposome, and (c) a NP-loaded liposome. Black lines represent Einstein's free diffusion law. The initial position of the particles is chosen randomly and the reported data in each of the figures are the average of more than 1000 different trajectories in a time duration of 1000 s. The average speckle intensity is increased from 1.08 to 5.46 $\mu W/\mu m^2$. In all cases, a transition from trapping at high speckle intensities to subdiffusion at low speckle intensities can be recognized.

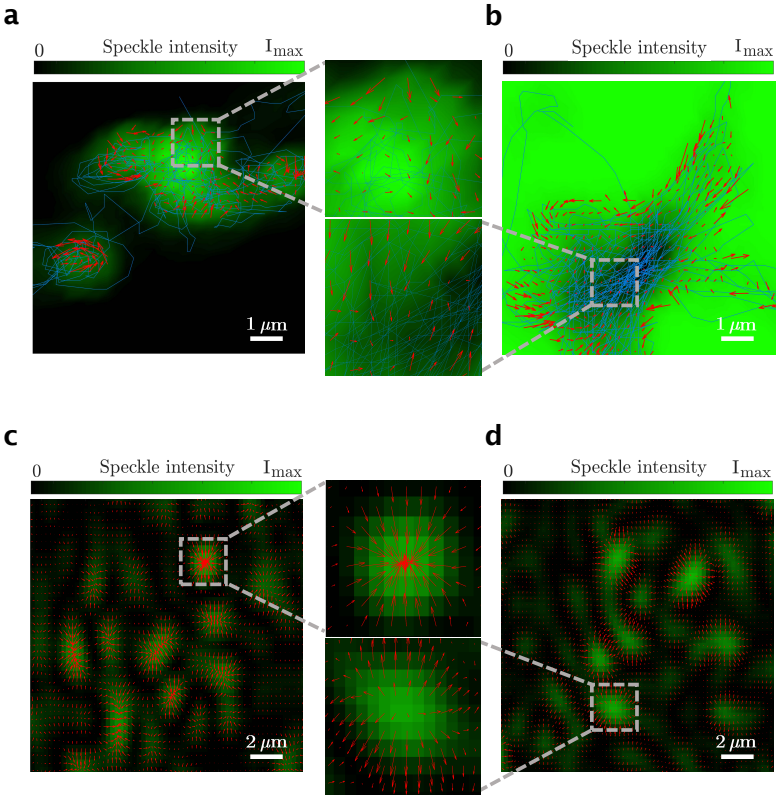

Fig. 4: Microscopic optical forces in a speckle field in the transversal plane for (a) a polystyrene (high-refractive-index, $n_p = 1.59$) and (b) a liposome vesicle (low-refractive-index, $n_l = 1.30$), reconstructed through the analysis of particle displacement information via the maximum-likelihood-estimator analysis method. (c) and (d) The corresponding simulated force fields in speckle fields of the same average intensity as in (a) and (b).

and partially transmitted, whose directions are different from those of the incoming rays. This change of direction causes a change of momentum and a force acting on the particle. Even if the geometrical optics approach can be employed when the characteristic dimensions of the object under study are significantly larger than the wavelength

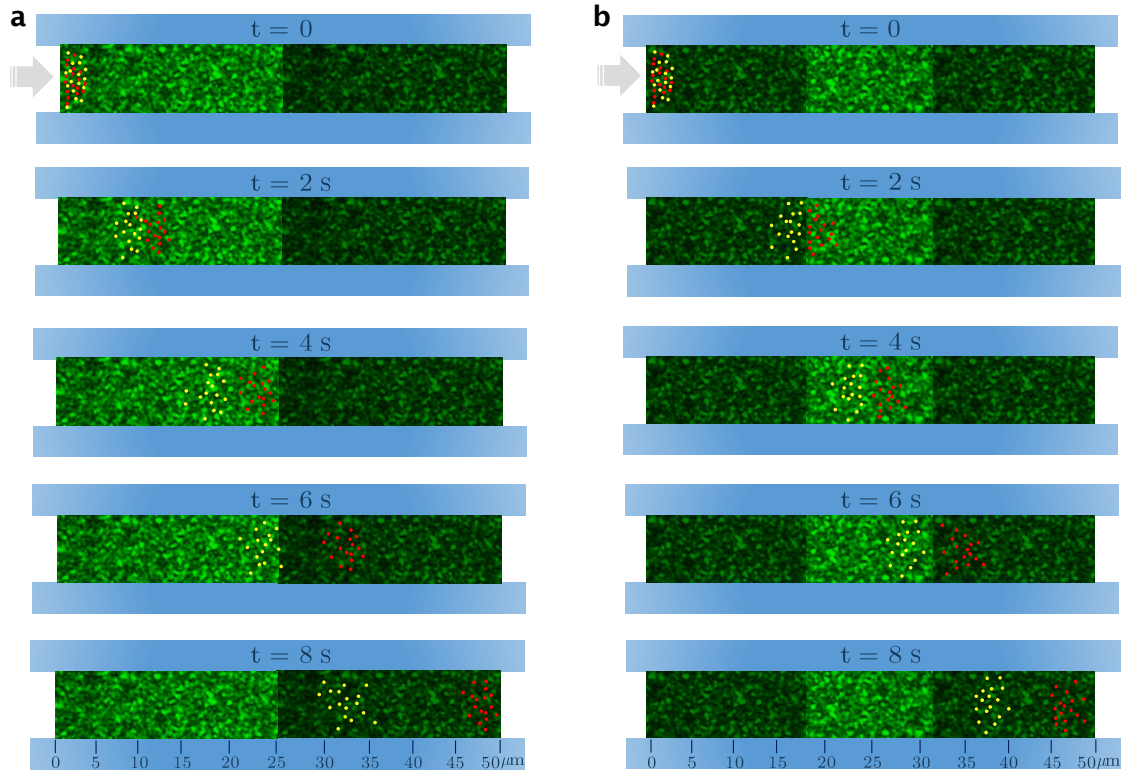

Fig. 5: Microfluidic speckle filtering of NP-loaded liposome (gold color dots) from the empty ones (red dots), based on their velocity hindering in varying speckle intensity. The average speckle intensity is changed (from $\langle I\rangle = 6.2\ \mu\text{W}/\mu\text{m}^2$ to $\langle I\rangle = 0.93\ \mu\text{W}/\mu\text{m}^2$, or vice versa) in (a) one, and (b) two boundaries. Sample time lapses belong to every 2 s and the process takes a time duration of about 8 s.

of the light, but it is shown that comparing to the calculations performed by use of more rigorous electromagnetic wave theory the ray optics results agree to within a factor of 2 even for particle radii as small as twice the incident wavelength [57]. The optical forces attract particles with high refractive index towards the intensity maxima of the optical field and repel the ones with low refractive index toward the minima. In Supplementary Fig. S4 for quantitative assessment, a set of points in the speckle field is randomly selected and their corresponding values for the optical potential in both low and high index (with respect to the surrounding) cases are presented in Table S1.

It is remarkable that besides to lateral sizes, a speckle grain in the speckle field has also an axial size. The typical axial size is calculated in the Supplementary file and schematically indicated in Supplementary Fig. S2. The particles are dispersed between the chamber upper and lower walls, and the optical scattering forces push the particles in the direction of light propagation towards the lower wall of the chamber. Therefore, the high refractive index (with respect to the surrounding) particles can be trapped within the grain axial longitude, so the speckle tweezers effectively confine the particles in a quasi two-dimensional space [43]. In case of low index (with respect to the surrounding) particle, however, the confinement is only in two dimensional space, since these particles are confined by dark regions.

In [43] G. Volpe et al. demonstrated that by employing a time-varying speckle pattern and via continuous control of the subdiffusion (a slope smaller than 1 in the MSD(Δt) function) to superdiffusion (a slope bigger than 1) transitions, it is possible to perform optical manipulation tasks such as guiding, sieving and sorting multiple particles. Indeed, compared to periodic potentials which are characterized by a few potential depths, ST represents a wider possibility (due to a distribution of intensities) to be operated for such tasks, provided that a controlling handle exists. However, controlling the variation of a produced speckle pattern comes along with challenges due to the inherent randomness of the speckle light fields. Nevertheless, the optical forces exerted on a particle depend on the particle's physical parameters, hence, a static speckle

pattern can be employed to realize a selection sieve in the presence of flow. A significant observation in this work is that for a flow of low-index particles (with respect to the surrounding) e.g. liposomes, the immediate effect of the presence of a speckle field is the reduction of their drift velocities. More importantly, for the liposomes inside which we loaded gold NPs, we observe that the reduction of the velocities is substantially increased. For these experiments, we use special chambers in which parts of one of the building walls are coated by a semi-transparent thin layer, therefore, it rejects partly the incident light. The coating thickness in Region 1 of case I and Region 2 of case II is 7 nm and the thickness in Region 2 of case I and Regions 1 and 3 of case II is 45 nm. The details of the chambers are explained in Supplementary Fig. S1. The rest of the uncoated area transmits almost all the light. In the chamber shown in Fig. 5**a** the right half of the coverslip is coated while in the one shown in Fig. 5**b** only the central part remains uncoated. Then a mixture suspension of empty liposomes and NP-loaded liposomes are injected into the chamber under a constant rate via a syringe pump and the flow is live monitored. Gold color and red dots represent the NP-loaded and empty liposomes, respectively. In Fig. 5, for both of the two aforementioned chambers it is demonstrated that microfluidic speckle filtering of NP-loaded liposomes from the empty ones is possible in a flow duration of a few seconds and within less than 50 μm range. The separation can be done because the NP-loaded liposomes drop behind with respect to the empty ones. Figure 5**a** shows that the presence of regions with different average intensities can tune the speed reduction difference, and, therefore, can boost the separation of the two sets of particles at the boundary of the regions. We demonstrate this type of control on the speed reduction difference further in Fig. 5**b** by adding another boundary which enables further control on the collective behavior of the flowing particles. This possibility to apply local changes on the average intensity over the speckle field makes is possible to design useful arrangements for directed collective motion of multiple particles.

In order to express the results in a more quantitative fashion, we track several particles during their flow and measure their velocities. Figure 6 summaries the results. As shown in Fig. 6**a**, in case I by coating a semi-transparent layer on a half of the chamber surface to reduce the transmittance of the laser light by 85%, two regions with average speckle intensity of $\langle I_{R1}\rangle = 6.2\ \mu\mathrm{W}/\mu\mathrm{m}^2$ (Region 1) and $\langle I_{R2}\rangle = 0.93\ \mu\mathrm{W}/\mu\mathrm{m}^2$ (Region 2) are achieved. In case II three regions of different average speckle intensity, $\langle I_{R1}\rangle = 0.93\ \mu\mathrm{W}/\mu\mathrm{m}^2$ (Region 1), $\langle I_{R2}\rangle = 6.2\ \mu\mathrm{W}/\mu\mathrm{m}^2$ (Region 2), and $\langle I_{R3}\rangle = 0.93\ \mu\mathrm{W}/\mu\mathrm{m}^2$ (Region 3) are existed. Figures 6**b,c** and 6**d-f** show the average velocity of 100 particles of each type for the first 8 s of experiments for the case I and case II, respectively. Blue dots and red squares indicate the velocities of empty liposomes and NP-loaded liposomes, respectively. For each experiment, a set of micro-particles at the same time is chosen. In Fig. 5 we show the positions of empty and NP-loaded liposomes of several experiments with red and yellow dots, respectively, at t= 0, 2 s, 4 s, 6 s, and 8 s. The particles are tracked in each frame, and their velocities are calculated between each two frame for successive frames, knowing the acquisition frame rate. The average velocities of each particle within 0.5 s are calculated. Then, these velocities are averaged over the values of the set of the particles. The results are the data points reported in Fig. 6**b-f**, and the errorbars are associated with the averaging over different particles. Supplementary videos S3 and S4 are related to the two arrangements in Fig. 5**a** and **b**. We also conduct a reference experiment, in which the laser is off and the speckle field is removed, therefore, the liposomes have the constant flowing speed along with the fluctuations caused by Brownian motion (black diamonds). It is obvious that both types of particles encounter velocity reduction. The decreasing of particle velocities originates form the point that micro-particles are trapped over longer times by a static speckle pattern. The hindering of velocities happens in multiple interacting of the particle and the speckle field. Between each two steps their Brownian motion and optical forces cause random motion so that they do not have sufficient free distance to reach to a constant speed. However, the reduction is substantially different for the NP-loaded and empty liposomes. The reduction is also different in different regions. These outcomes are shown by the difference in the slopes of the fitted lines to the data. In Fig. 6**b** the lines fitted to velocities of the empty liposomes (blue line) and the NP-loaded liposomes (red line) in the initial seconds (moving in Region 1) have the slopes of $m_{L,R1} = -0.85\ \mu\mathrm{m/s}^2$ and $m_{NP,R1} = -1.22\ \mu\mathrm{m/s}^2$, respectively. When the particles cross the boundary of the two regions of case I (Fig. 6**c**) the decrease of the velocities of both types in Region 2 follows a different trend ($m_{L,R2} = -0.30\ \mu\mathrm{m/s}^2$ and $m_{NP,R2} = -0.38\ \mu\mathrm{m/s}^2$). For the case II the trends of the same order in velocity reduction of empty and NP-loaded liposomes are measured in the Regions 1 and 3, which have similar average speckle intensity ($m_{L,R1} = -0.34\ \mu\mathrm{m/s}^2$, $m_{L,R3} = -0.20\ \mu\mathrm{m/s}^2$ and $m_{NP,R1} = -0.54\ \mu\mathrm{m/s}^2$, $m_{NP,R3} = -0.30\ \mu\mathrm{m/s}^2$). However, the velocity in Region 2 which has higher average speckle intensity decreases dramatically ($m_{L,R2} = -0.99\ \mu\mathrm{m/s}^2$ and $m_{NP,R2} = -1.18\ \mu\mathrm{m/s}^2$). The use of different regions with different mean intensities is an ex-

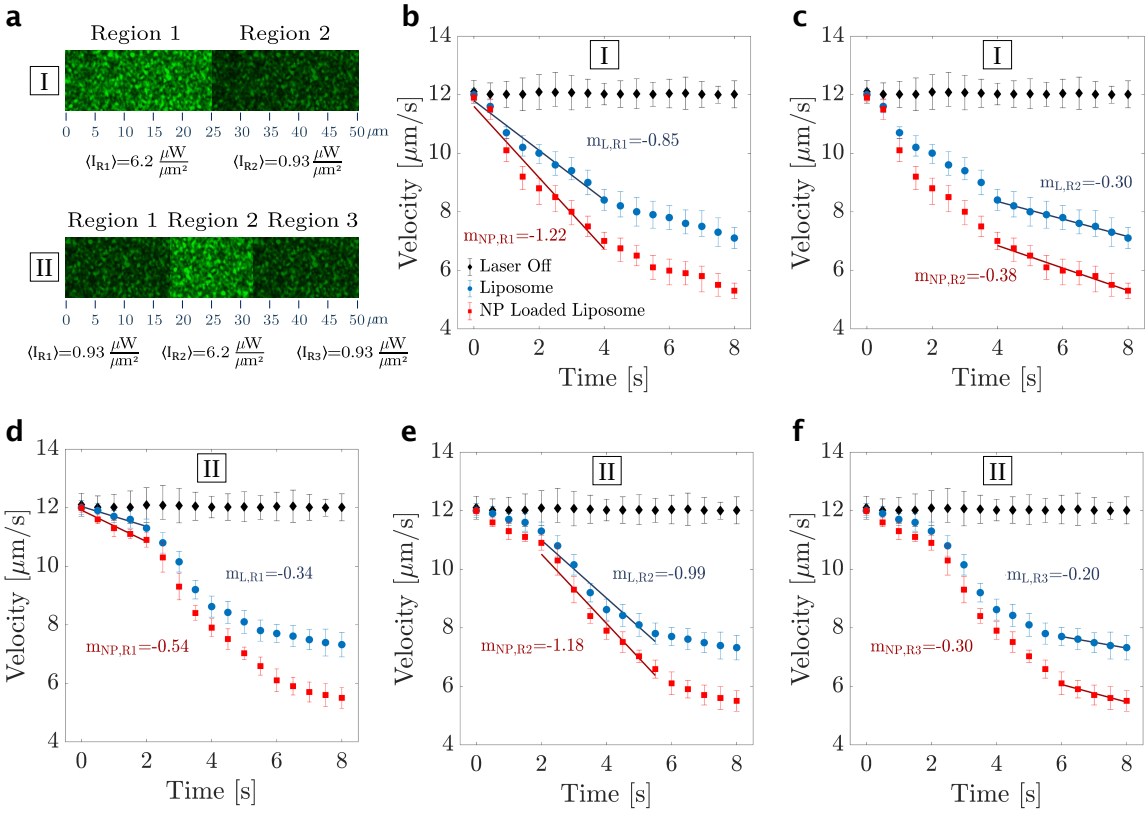

Fig. 6: (a) Case I: the chamber surfaces is half-coated by a semi-transparent layer to reduce the transmittance of the laser light by 85% in Region 2, and Case II: two-third of of the chamber surface is coated (Regions 2 and 3). (b) and (c) The average velocity of empty (blue dots) and NP-loaded (red squares) liposomes and their associated fitted lines in Regions 1 (panel b) and 2 (panel c) of case I. (d-f) The average velocity of empty and NP-loaded liposomes and their associated fitted lines in Regions 1 (panel d), 2 (panel e) and 3 (panel f) of case II. The slope of the fitted lines are in $\mu m/s^2$ units. The black diamonds represent the velocity of a liposome when the speckle generating laser is off, as a reference experiment.

ample of incorporating additional intensity gradient to perform adjustable space-time-varying fields, which enhances the capability of the speckle tweezers applications. For example, in Fig. 5**a**, it can be seen that when the empty liposomes reach to the boundary of the two regions (at t= 6 s) their motion experiences a boost so that the NP-loaded liposomes drop behind further, making their separation more feasible.

The NP-loaded liposomes drop behind the empty ones when they pass through a speckle field. However, the presence of regions with different average intensities substantially enhances the separation procedure. For example, in Fig. 5**a**, let us compare the movement of the particles for the duration of t=2 s to t= 4 s and the duration of t=6 s to t=8 s, in which the particles experience the boundary between the regions of different average intensities. The empty liposomes from t= 2 s to t= 4 s move from d≈ 12μm to d≈ 22μm, and the NP-loaded liposomes move from d≈ 10μm to d≈ 17μm. However, from t= 6 s to t= 8 s the empty liposomes move from d≈ 32μm to d≈ 50μm, and the NP-loaded liposomes move from d≈ 24μm to d≈ 33μm. Since the other experimental conditions are preserved, the substantial difference between the behaviors is attributed to the presence of the regions of different average intensities. It is obvious that more than 30% of the velocity reduction difference between the empty and NP-loaded liposomes in a few seconds, which is deduced from our results, is sufficient to separate out the two important classes of the particles. The separation can be followed by guiding the first outgoing particles into a specific reservoir as no NP-loaded ones. In this example, the advantage of the presence of the boundary is the enhanced separation between the empty and the NP-loaded liposomes. In general, the additional control on the local speckle areas, especially if several regions of different average intensities are considered, will increase significantly the capability of ST applications. Proper geometry of the fluidic channels and controlled speckle field

engineering can be also combined toward the application of the method in endoscopic studies. It is remarkable that the hydrodynamic interactions between dispersed particles induced with the speckle field, cause the changes in their particle-particle distances and can hinder their diffusion [59–61]. However, this effect is common for either NP encapsulated or empty liposomes and can be disregarded in the presented experiment schemes.

The difference between the velocity reduction of NP-loaded and empty liposomes may be explained by the inclusion of the photophoretic forces on NPs. Photophoretic force is the result of thermal processes caused by the absorption of laser light by the particles. Therefore, in the optical force calculation for metallic NPs, either entrapped inside bubbles or freely moving, the effect of the local electromagnetic fields and the photophoretic forces have to be considered [62]. The theoretical investigation of the applied forces for irregularly shaped particles or irregularly distributed laser fields can be performed by the T-matrix method [63]. However, quantitative consideration of the photophoretic force on an absorbing particle involves many factors, such as pressure, light properties e.g. beam profile, intensity, wavelength, and polarizations, and particle properties e.g. size, geometrical shape, and thermal conductivity [63, 64]. The effects can be either a pushing or pulling force. It has been already shown that airborne metallic NPs may be trapped in the dark regions of speckle fields [62]. Here, similarly, the photophoretic trapping partially holds the NPs, therefore, and it hinders the associated liposomes velocities. The Supplementary video S5 shows the behavior of a NP-loaded liposome in a quiescent fluid under illumination of speckle fields of different average intensities, which validates the predicted confinement in dark regions of the speckle fields. In Supplementary Fig. S3 a schematic figure to show the acting forces in different cases (high index, low index and NP-loaded low index particles) is presented.

Gold NP, itself, can enter liposome and be used as a drug. Moreover, NP-loaded liposome can resemble drug-loaded containers in drug delivery, in general. Therefore, this platform along with easy handling of speckle fields can provide an elegant approach for controlling the drug-loaded containers, for example for collective manipulation of transfection reagents, cell markers, and carriers of molecules [65].

Various size ranges of high refractive index particles have been subjected to manipulation by speckle fields [43, 66]. For example, in [43] sub-micron polystyrene particles of different diameters and refractive indices are sieved by passing through the speckle field. For the low refractive index particles, due to the topological structure of speckle field, which contains a tunable distribution of isolated high-intensity regions surrounded by interconnected low-intensity regions [52], we believe that, on the one hand, even larger ranges of particles can be manipulated by the dark regions. On the hand, for smaller sizes, especially the metallic particles, these light fields can perform a large-scale filtration by opto-thermoelectric speckle tweezers [46]. The physics behind is that for the smaller metallic particles the thermoelectric force is dominant. This method of filtration of nanoparticles aggregations in complex fluids can be an alternative to high speed centrifuging.

4 Conclusions

In conclusion, we extend the usefulness of speckle tweezers into low refractive index micro-particles and reported different particle speckle field interaction between empty and nano-particle loaded vesicles. The speckle fields have great potential to collectively guide, select, trap, or push micro-particles of low- and high- refractive-index with respect to their surrounding. The high-intensity regions of the speckle fields can act as a size selection sieve for dielectric particles of high-refractive-index. On the other hand, and more importantly, the low-intensity regions of the speckle fields can perform the aforementioned tasks through the size selection sieve for dielectric particles of low-refractive-index (with respect to the surrounding) , or through a photophoretic sieve for absorptive ones, whether embedded inside the containers or not. The rather low average intensity throughout the field that illuminates the samples can be considered as another profitable feature of the methodology. Furthermore, in addition to the inherent irregular structure of the speckle field, by proper patterning the sample chamber, it is also possible to adjust the average intensity of the field covering an area over the sample or apply an additional intensity gradient, i.e., perform space-time-varying fields. Therefore, dynamic control can be applied to the samples with the important advantages of ST over the typical regular pattern of trapping sites. The requirement to only a few optical components and saving physical space, insensitivity to optical aberrations, use of unfocused light, and no need for sophisticated alignment and adjustment processes, are some of the ST advantages. These benefits and their compatibility with out of the physics laboratory and in-vivo situations make ST a simple, cost-effective, and versatile methodology for applications in various fields, such as drug delivery, lab-on-a-chip, and active matter. We believe that the principal idea behind the applications of the optical ST can also be

extended to acoustical trapping, which has very recently attracted intensive attention [67–69].

Acknowledgment: The authors would like to thank Saeed Mollaei and Mohammad-Reza Aghdaei for their assistance in performing the experiments, and Bahman Farnudi for linguistic editing of the manuscript.

Conflict of Interest: The authors declare no conflicts of interest regarding this article.

References

[1] D. G. Grier, "A revolution in optical manipulation," *Nature*, vol. 424, no. 6950, pp. 810–816, 2003.

[2] C. Hertlein, L. Helden, A. Gambassi, S. Dietrich, and C. Bechinger, "Direct measurement of critical casimir forces," *Nature*, vol. 451, no. 7175, pp. 172–175, 2008.

[3] J. Munday and F. Capasso, "Repulsive casimir and van der waals forces: From measurements to future technologies," *International Journal of Modern Physics A*, vol. 25, no. 11, pp. 2252–2259, 2010.

[4] P. v. Tien, "Light waves in thin films and integrated optics," *Applied Optics*, vol. 10, no. 11, pp. 2395–2413, 1971.

[5] G. S. Campbell and J. Norman, *An introduction to environmental biophysics*. Springer Science & Business Media, 2012.

[6] D. S. Wiersma, "Disordered photonics," *Nature Photonics*, vol. 7, no. 3, pp. 188–196, 2013.

[7] S. Rotter and S. Gigan, "Light fields in complex media: Mesoscopic scattering meets wave control," *Reviews of Modern Physics*, vol. 89, no. 1, p. 015005, 2017.

[8] G. Jacucci, L. Schertel, Y. Zhang, H. Yang, and S. Vignolini, "Light management with natural materials: From whiteness to transparency," *Advanced Materials*, p. 2001215, 2020.

[9] D. S. Wiersma and S. Cavalieri, "A temperature-tunable random laser," *Nature*, vol. 414, no. 6865, pp. 708–709, 2001.

[10] B. Redding, S. F. Liew, R. Sarma, and H. Cao, "Compact spectrometer based on a disordered photonic chip," *Nature Photonics*, vol. 7, no. 9, p. 746, 2013.

[11] M. Eichenfield, C. P. Michael, R. Perahia, and O. Painter, "Actuation of micro-optomechanical systems via cavity-enhanced optical dipole forces," *Nature Photonics*, vol. 1, no. 7, p. 416, 2007.

[12] A. Grigorenko, N. Roberts, M. Dickinson, and Y. Zhang, "Nanometric optical tweezers based on nanostructured substrates," *Nature Photonics*, vol. 2, no. 6, pp. 365–370, 2008.

[13] J. Shi, D. Ahmed, X. Mao, S.-C. S. Lin, A. Lawit, and T. J. Huang, "Acoustic tweezers: patterning cells and microparticles using standing surface acoustic waves (ssaw)," *Lab on a Chip*, vol. 9, no. 20, pp. 2890–2895, 2009.

[14] D. Fan, F. Zhu, R. Cammarata, and C. Chien, "Electric tweezers," *Nano Today*, vol. 6, no. 4, pp. 339–354, 2011.

[15] J. Nilsson, M. Evander, B. Hammarström, and T. Laurell, "Review of cell and particle trapping in microfluidic systems," *Analytica chimica acta*, vol. 649, no. 2, pp. 141–157, 2009.

[16] M. F. Yanik, C. B. Rohde, and C. Pardo-Martin, "Technologies for micromanipulating, imaging, and phenotyping small invertebrates and vertebrates," *Annual review of biomedical engineering*, vol. 13, pp. 185–217, 2011.

[17] S. Ghosh and A. Ghosh, "Mobile nanotweezers for active colloidal manipulation," *Science Robotics*, vol. 3, no. 14, p. eaaq0076, 2018.

[18] E. Spyratou, M. Makropoulou, E. Mourelatou, and C. Demetzos, "Biophotonic techniques for manipulation and characterization of drug delivery nanosystems in cancer therapy," *Cancer Letters*, vol. 327, no. 1-2, pp. 111–122, 2012.

[19] A. Ashkin, "Acceleration and trapping of particles by radiation pressure," *Physical Review Letters*, vol. 24, no. 4, p. 156, 1970.

[20] P. Verkerk, B. Lounis, C. Salomon, C. Cohen-Tannoudji, J.-Y. Courtois, and G. Grynberg, "Dynamics and spatial order of cold cesium atoms in a periodic optical potential," *Physical review letters*, vol. 68, no. 26, p. 3861, 1992.

[21] S. Haroche, "Nobel lecture: Controlling photons in a box and exploring the quantum to classical boundary," *Reviews of Modern Physics*, vol. 85, no. 3, p. 1083, 2013.

[22] J. E. Curtis, B. A. Koss, and D. G. Grier, "Dynamic holographic optical tweezers," *Optics Communications*, vol. 207, no. 1-6, pp. 169–175, 2002.

[23] D. Gao, W. Ding, M. Nieto-Vesperinas, X. Ding, M. Rahman, T. Zhang, C. Lim, and C.-W. Qiu, "Optical manipulation from the microscale to the nanoscale: fundamentals, advances and prospects," *Light: Science & Applications*, vol. 6, no. 9, pp. e17039–e17039, 2017.

[24] M. Miyazaki and Y. Hayasaki, "Motion control of low-index microspheres in liquid based on optical repulsive force of a focused beam array," *Optics Letters*, vol. 34, no. 6, pp. 821–823, 2009.

[25] F. Peng, B. Yao, S. Yan, W. Zhao, and M. Lei, "Trapping of low-refractive-index particles with azimuthally polarized beam," *JOSA B*, vol. 26, no. 12, pp. 2242–2247, 2009.

[26] P. Prentice, M. MacDonald, T. Frank, A. Cuschieri, G. Spalding, W. Sibbett, P. Campbell, and K. Dholakia, "Manipulation and filtration of low index particles with holographic laguerre-gaussian optical trap arrays," *Optics Express*, vol. 12, no. 4, pp. 593–600, 2004.

[27] P. H. Jones, E. Stride, and N. Saffari, "Trapping and manipulation of microscopic bubbles with a scanning optical tweezer," *Applied physics letters*, vol. 89, no. 8, p. 081113, 2006.

[28] P. Jones, O. Maragó, and E. Stride, "Parametrization of trapping forces on microbubbles in scanning optical tweezers," *Journal of Optics A: Pure and Applied Optics*, vol. 9, no. 8, p. S278, 2007.

[29] R. Dasgupta, S. Ahlawat, R. S. Verma, S. Shukla, and P. K. Gupta, "Optical trapping of spermatozoa using laguerre-gaussian laser modes," *Journal of biomedical optics*, vol. 15, no. 6, p. 065010, 2010.

[30] S. Putterman, P. Evans, G. Vazquez, and K. Weninger, "Is there a simple theory of sonoluminescence?," *Nature*, vol. 409, no. 6822, pp. 782–783, 2001.

[31] N. De Jong, A. Bouakaz, and P. Frinking, "Basic acoustic properties of microbubbles," *Echocardiography*, vol. 19, no. 3, pp. 229–240, 2002.
[32] J. Y. Ye, G. Chang, T. B. Norris, C. Tse, M. J. Zohdy, K. W. Hollman, M. O'Donnell, and J. R. Baker, "Trapping cavitation bubbles with a self-focused laser beam," *Optics Letters*, vol. 29, no. 18, pp. 2136–2138, 2004.
[33] D. E. Discher and A. Eisenberg, "Polymer vesicles," *Science*, vol. 297, no. 5583, pp. 967–973, 2002.
[34] S. Mohanty, R. Verma, and P. Gupta, "Trapping and controlled rotation of low-refractive-index particles using dual line optical tweezers," *Applied Physics B*, vol. 87, no. 2, pp. 211–215, 2007.
[35] K. Tachibana, T. Uchida, K. Ogawa, N. Yamashita, and K. Tamura, "Induction of cell-membrane porosity by ultrasound," *The Lancet*, vol. 353, no. 9162, p. 1409, 1999.
[36] L. Zarif, "Drug delivery by lipid cochleates," in *Methods in enzymology*, vol. 391, pp. 314–329, Elsevier, 2005.
[37] P. M. Hansen, V. K. Bhatia, N. Harrit, and L. Oddershede, "Expanding the optical trapping range of gold nanoparticles," *Nano Letters*, vol. 5, no. 10, pp. 1937–1942, 2005.
[38] G. Rui, X. Wang, and Y. Cui, "Manipulation of metallic nanoparticle with evanescent vortex bessel beam," *Optics Express*, vol. 23, no. 20, pp. 25707–25716, 2015.
[39] K. Gahagan and G. Swartzlander, "Simultaneous trapping of low-index and high-index microparticles observed with an optical-vortex trap," *JOSA B*, vol. 16, no. 4, pp. 533–537, 1999.
[40] Z. Liu, X. Tang, Y. Zhang, Y. Zhang, L. Ma, M. Zhang, X. Yang, J. Zhang, J. Yang, and L. Yuan, "Simultaneous trapping of low-index and high-index microparticles using a single optical fiber bessel beam," *Optics and Lasers in Engineering*, vol. 131, p. 106119, 2020.
[41] J.-P. Bouchaud and A. Georges, "Anomalous diffusion in disordered media: statistical mechanisms, models and physical applications," *Physics Reports*, vol. 195, no. 4-5, pp. 127–293, 1990.
[42] J. W. Goodman, *Speckle phenomena in optics: theory and applications*. Roberts and Company Publishers, 2007.
[43] G. Volpe, G. Volpe, and S. Gigan, "Brownian motion in a speckle light field: tunable anomalous diffusion and selective optical manipulation," *Scientific Reports*, vol. 4, p. 3936, 2014.
[44] V. G. Shvedov, A. V. Rode, Y. V. Izdebskaya, A. S. Desyatnikov, W. Krolikowski, and Y. S. Kivshar, "Selective trapping of multiple particles by volume speckle field," *Optics express*, vol. 18, no. 3, pp. 3137–3142, 2010.
[45] M. V. Chubynsky and G. W. Slater, "Diffusing diffusivity: a model for anomalous, yet brownian, diffusion," *Physical Review Letters*, vol. 113, no. 9, p. 098302, 2014.
[46] A. Kotnala, P. S. Kollipara, and Y. Zheng, "Opto-thermoelectric speckle tweezers," *Nanophotonics*, vol. 9, no. 4, pp. 927–933, 2020.
[47] A. S. Nunes, S. K. Velu, I. Kasianiuk, D. Kasyanyuk, A. Callegari, G. Volpe, M. M. T. da Gama, G. Volpe, and N. A. Araújo, "Ordering of binary colloidal crystals by random potentials," *Soft Matter*, vol. 16, no. 17, pp. 4267–4273, 2020.
[48] E. Pinçe, S. K. Velu, A. Callegari, P. Elahi, S. Gigan, G. Volpe, and G. Volpe, "Disorder-mediated crowd control in an active matter system," *Nature Communications*, vol. 7, no. 1, pp. 1–8, 2016.
[49] M. Recanello, E. Lenzi, A. Martins, Q. Li, and R. Zola, "Extended adsorbing surface reach and memory effects on the diffusive behavior of particles in confined systems," *International Journal of Heat and Mass Transfer*, vol. 151, p. 119433, 2020.
[50] I. Freund, "'1001' correlations in random wave fields," *Waves in random media*, vol. 8, no. 1, pp. 119–158, 1998.
[51] M. Berry and M. Dennis, "Phase singularities in isotropic random waves," *Proceedings of the Royal Society of London. Series A: Mathematical, Physical and Engineering Sciences*, vol. 456, no. 2001, pp. 2059–2079, 2000.
[52] J. Gâteau, F. Claude, G. Tessier, and M. Guillon, "Topological transformations of speckles," *Optica*, vol. 6, no. 7, pp. 914–920, 2019.
[53] B. Maherani, E. Arab-Tehrany, M. R Mozafari, C. Gaiani, and M. Linder, "Liposomes: a review of manufacturing techniques and targeting strategies," *Current Nanoscience*, vol. 7, no. 3, pp. 436–452, 2011.
[54] N. Bender, H. Yılmaz, Y. Bromberg, and H. Cao, "Customizing speckle intensity statistics," *Optica*, vol. 5, no. 5, pp. 595–600, 2018.
[55] L. P. García, J. D. Pérez, G. Volpe, A. V. Arzola, and G. Volpe, "High-performance reconstruction of microscopic force fields from brownian trajectories," *Nature Communications*, vol. 9, no. 1, pp. 1–9, 2018.
[56] Y. Shimoni, G. Nudelman, F. Hayot, and S. C. Sealfon, "Multi-scale stochastic simulation of diffusion-coupled agents and its application to cell culture simulation," *PloS One*, vol. 6, no. 12, 2011.
[57] L. P. García, J. D. Pérez, G. Volpe, A. V. Arzola, and G. Volpe, "High-performance reconstruction of microscopic force fields from brownian trajectories," *Figshare https://doi.org/10.6084/m9.figshare.7181888*, no. 1, 2018.
[58] A. Callegari, M. Mijalkov, A. B. Gököz, and G. Volpe, "Computational toolbox for optical tweezers in geometrical optics," *JOSA B*, vol. 32, no. 5, pp. B11–B19, 2015.
[59] J. P. Segovia-Gutiérrez, M. A. Escobedo-Sánchez, E. Sarmiento-Gómez, and S. U. Egelhaaf, "Diffusion of anisotropic particles in random energy landscapes-an experimental study," *Frontiers in Physics*, vol. 7, p. 224, 2019.
[60] R. D. Hanes, M. Schmiedeberg, and S. U. Egelhaaf, "Brownian particles on rough substrates: Relation between intermediate subdiffusion and asymptotic long-time diffusion," *Physical Review E*, vol. 88, no. 6, p. 062133, 2013.
[61] R. Pastore, A. Ciarlo, G. Pesce, F. Greco, and A. Sasso, "Rapid fickian yet non-gaussian diffusion after subdiffusion," *Physical Review Letters*, vol. 126, no. 15, p. 158003, 2021.
[62] K. L. Kelly, E. Coronado, L. L. Zhao, and G. C. Schatz, "The optical properties of metal nanoparticles: the influence of size, shape, and dielectric environment," 2003.
[63] A. Jonáš and P. Zemanek, "Light at work: The use of optical forces for particle manipulation, sorting, and analysis," *Electrophoresis*, vol. 29, no. 24, pp. 4813–4851, 2008.
[64] V. G. Shvedov, C. Hnatovsky, N. Eckerskorn, A. V. Rode, and W. Krolikowski, "Polarization-sensitive photophoresis," *Applied Physics Letters*, vol. 101, no. 5, p. 051106, 2012.
[65] A. Lehmuskero, P. Johansson, H. Rubinsztein-Dunlop, L. Tong, and M. Kall, "Laser trapping of colloidal metal

nanoparticles," *ACS Nano*, vol. 9, no. 4, pp. 3453–3469, 2015.

[66] G. Volpe, L. Kurz, A. Callegari, G. Volpe, and S. Gigan, "Speckle optical tweezers: micromanipulation with random light fields," *Optics express*, vol. 22, no. 15, pp. 18159–18167, 2014.

[67] K. Dholakia, B. W. Drinkwater, and M. Ritsch-Marte, "Comparing acoustic and optical forces for biomedical research," *Nature Reviews Physics*, vol. 2, no. 9, pp. 480–491, 2020.

[68] A. Marzo and B. W. Drinkwater, "Holographic acoustic tweezers," *Proceedings of the National Academy of Sciences*, vol. 116, no. 1, pp. 84–89, 2019.

[69] D. Baresch and V. Garbin, "Acoustic trapping of microbubbles in complex environments and controlled payload release," *Proceedings of the National Academy of Sciences*, vol. 117, no. 27, pp. 15490–15496, 2020.